IEEE Access
Multidisciplinary | Rapid Review | Open Access Journal

Received March 14, 2021, accepted March 16, 2021, date of publication March 23, 2021, date of current version March 30, 2021.

Digital Object Identifier 10.1109/ACCESS.2021.3068082

Design and Experimental Analysis of a Novel Compact and Flexible Super Wide Band Antenna for 5G

SHUVASHIS DEY, (Member, IEEE), MD SHAMSUL AREFIN, AND NEMAI CHANDRA KARMAKAR, (Senior Member, IEEE)
Department of Electrical and Computer Systems Engineering, Monash University, Clayton, VIC 3800, Australia
Corresponding author: Shuvashis Dey (shuvashis.dey@monash.edu)

This work was supported by the Australian Research Council Discovery Project under Grant DP110105606.

ABSTRACT This paper investigates the design and practical implementation of a novel Super Wide Band (SWB) antenna on a flexible substrate. The antenna is designed on the Ultralam 3850 substrate having a compact dimension of $60 \times 40 \times 0.1$ mm^3. This antenna has an operating frequency band from 1.74 to 100 GHz with a bandwidth (BW) ratio of approximately 57.47:1. Such an extended frequency coverage makes this antenna operable in a wide variety of wireless application areas, including 5G and the Internet of Things (IoT). The simulated performance of the designed antenna is analyzed here with respect to different antenna parameters, including reflection coefficient, radiation pattern, gain, efficiency, and surface current. The proposed antenna prototype is fabricated, and experimental validation is provided through the measurement using a programmable network analyzer (PNA).

INDEX TERMS Super Wide Band, SWB, WBAN, IoT, ratio bandwidth (BW), mmWave, LTE, 5G, massive MIMO, textile antenna, advanced antenna systems (AAS).

I. INTRODUCTION

Owing to the remarkable development of wireless communication, there has been an increasing trend of growing network and data traffic. To comply with this demand, the fifth generation (5G) wireless system is being deployed, which can offer an enhanced frequency spectrum and unprecedented data rates as high as multi-Gigabit per second (Gbps) [1]. 5G technology would use the existing 4G band along with the newly defined 5G frequency ranges, including millimeter-wave (mmWave) bands (26, 28, 40, 50, and 66 GHz) [2], [3]. 5G communication systems will have the ability to support the Internet of Things (IoT) applications, and therefore IoT devices need to be 5G enabled [4]. This requirement, along with the usage of mmWave applications, instigate the necessity of integrating small-sized enhanced bandwidth (BW) antennas in 5G communication devices [5].

An antenna is one of the most crucial parts of any radio communication platform. Evolution in communication electronics has made it easier to develop compact, reliable, and advanced antenna systems (AAS) [6], [7]. Since the emergence of RF (radio frequency) communication, there has been an ever-increasing demand for compact and ubiquitous antennas. The modern-day communication systems require versatile multi-antenna technologies, which further escalates the necessity for small mobile terminals. Such small-scale equipment, including cellular phones, navigation devices, radio frequency identification (RFID) tag or sensors, as well as connected IoT and 5G devices, instigate the adoption of pervasive, high data capacity antennas with increased bandwidth. The widespread use of such devices and the constant growth of mobile network technology will continue to challenge researchers to design and develop compact, high performance, and cost-effective AAS on an ongoing basis [8], [9].

Ultra-Wide Band (UWB) is a radio communication protocol that can use low power to offer short-range connectivity with an increased data rate. This technology is beneficial for a wide range of applications, including multimedia services, home networking, medical, wireless personal area network (WPAN), and many others. However, due to its universal applicability through both short and long-distance data communication, in recent years, the super wideband (SWB)

The associate editor coordinating the review of this manuscript and approving it for publication was Giorgio Montisci.

technology has drawn an increased amount of attention [10]. This technology includes all the sophisticated features of UWB. Besides, compared to that of the UWB, it offers better channel capacity with a higher data rate and an increased resolution [11]. SWB implies a ratio bandwidth equals to or greater than 10:1, which means a broader frequency range than the decade bandwidth [12]. SWB antennas can be designed to occupy a very high bandwidth, which can cover most of the existing and proposed frequency bands specified for 5G applications. These antennas can also facilitate the wireless body area network (WBAN) applications by incorporating low-cost, flexible designs. WBAN requires wearable wideband antennas that can exchange digital information by using the human body as a data network [13]. To ensure the comfort of users, such on-body antennas need to be designed on flexible textile or plastic substrates.

This paper illustrates the design and analysis of a novel compact SWB antenna on a flexible substrate material. The designed antenna operating band covers more than 98 GHz with a frequency range from 1.74 to 100 GHz, and therefore it can be said to have an SWB frequency range. The SWB antenna has a bandwidth ratio of 57.47:1, and it covers most of the current and prospective 5G frequency bands under consideration. The proposed design comprises a monopole antenna with a small and thinner structure. The antenna is devised on a low-cost commercial substrate ULTRALAM 3850 laminate [14]. Here, the EM solver software CST Microwave (MW) Studio is used to perform the entire design and simulation. The designed antenna prototype is fabricated, and a thorough measured analysis is carried out to provide an experimental validation. A programmable network analyzer (PNA) with a maximum range of 67 GHz is utilized to perform this measurement. A thorough investigation of frequency response, radiation characteristics, and surface current is conducted to demonstrate that the simulated and measured results conform well with each other.

The structure of this paper is as follows: Section II provides a literature survey of the SWB antenna-based research articles, while section III introduces the design and operating principle of the proposed SWB antenna. Section IV illustrates the details of simulated results, and section V portrays the analysis of experimental results obtained from the practically fabricated antenna prototype. The proposed antenna's applicability for 5G is depicted in section VI, followed by the conclusions and future directions in section VII.

II. RELATED WORKS

A wide variety of antenna design approaches and procedures are implemented to obtain super wideband operation. A careful review of the literature shows that recently there has been a growing interest in SWB antenna-based research in the antenna community [10]–[12], [15]–[30]. An antenna that occupies the SWB range of 1.44-18.8 GHz is depicted in [10]. It can effectively cover many of the commonly used technological areas that are based on wireless communication such as Universal Mobile Telecommunication System (UMTS), Long term evolution (LTE), Bluetooth, Personal Communication System (PCS), WiMAX, Digital Cellular System (DCS) and UWB. However, this antenna does not suit high-frequency applications such as mmWave. In [29], a planar compact SWB antenna has been proposed, which operates from 20-120 GHz and therefore covers the mmWave and massive multiple input multiple output (MIMO) applications for 5G. However, this antenna is not experimentally validated, and it fails to perform at the low frequency 5G bands. Another low-profile wideband MIMO antenna for 5G smartphones is illustrated in [31], although it is quite a band-specific antenna that does not fall in the definition of SWB. In [12], [32], super wideband antennas on flexible substrates and their performance analysis under bending conditions are illustrated. Tran *et al.* proposed a functional section design (FSD) approach-based SWB antenna that has an operating bandwidth from 5 to 150 GHz [11], [17]. Although this antenna has an extensive frequency band, it is not a good fit for the low-frequency applications that entail S and L-band communications along with lower 5G frequency ranges. A circular-hexagonal geometry-based fractal antenna is presented in [18]. With a compact dimension of 31 $\times$ 45 mm^2, this antenna offers an SWB band of 2.18 - 44.5 GHz. However, it fails to operate in a range of widely used bands in the wireless spectrum, including UMTS, global positioning systems (GPS), L-band, DCS, and PCS. Another SWB antenna with an extremely wideband is proposed [19]. This compact directional antenna can operate in the frequency band of 11-200 GHz. Nonetheless, the performance of this antenna is not experimentally validated, and it does not cover the low and mid-band 5G applications [3]. A closer look at the SWB antenna-based published articles signifies that the reported antenna in [28] debatably offers the maximum ratio bandwidth (63.3:1) obtained to date. The antenna presented in [23] reports having a bandwidth ratio of 111.1:1, yet this antenna has a notched band of 4.7-6 GHz, which restrains its uninterrupted SWB coverage. In [33], the authors proposed a circular monopole-based SWB antenna that exhibits a visual resemblance to the one proposed in this work. However, the specified antenna is designed on a thick and rigid substrate, which restrains its applicability as a flexible antenna for WBAN and other conformal applications. The proposed antenna in this paper has different substrate properties and dimensions compared to the published work in [33]. Therefore, it requires a completely different feed network and ground perturbation to obtain impedance matching over its occupied bandwidth. In [34], Balani *et al.* have presented an exhaustive review of the super wideband antennas available in the literature. This review provides a comparative insight into the existing antennas based on a range of performance characteristics. The proposed antenna presented in this article has excellent suitability for a diversified range of wireless application areas, including UMTS, UWB, Bluetooth, 4G LTE, WBAN, 5G mmWave, and most of the prospective 5G low and mid-band-based applications. This antenna also covers the S, C, X, Ku, K, Ka, and Q bands, and therefore,

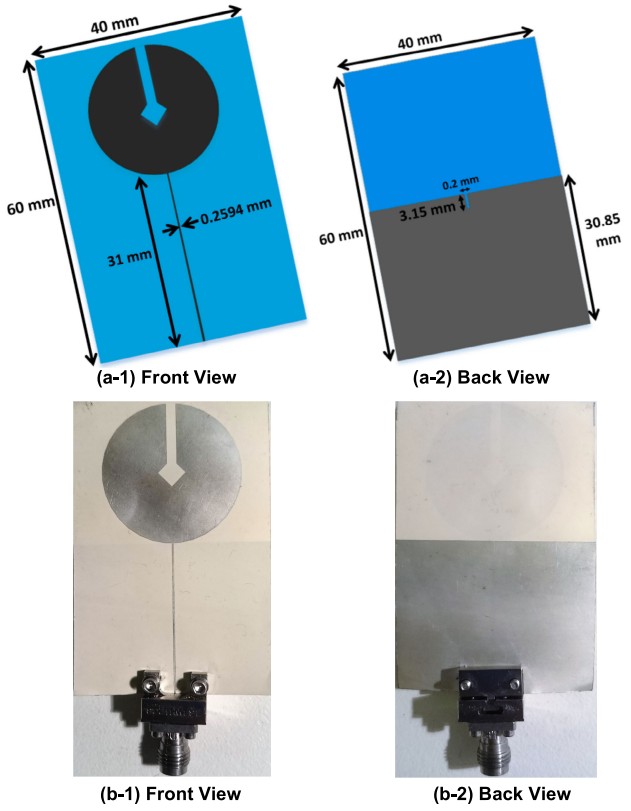

FIGURE 1. Antenna on Ultralam 3850 laminate with a patch thickness of 0.018 mm (18 um) (a) Simulated (b) Fabricated.

it has applicability in radio astronomy and satellite communications [35]. It supports the bands (45 GHz and 60 GHz) of the recently approved IEEE 802.11aj standard as well. These bands offer an increased network capacity by enabling low-powered devices to provide an extensive coverage area with a data rate of up to 15 Gbps [36], [37].

III. ANTENNA DESIGN AND OPERATIONAL MECHANISM

This section portrays the design of the proposed compact and flexible SWB antenna based on a circular disc monopole. The lightweight and low-profile characteristics of this antenna enable easy integration with the substrate. Fig. 1 (a) and (b) show the designed and fabricated antenna on ULTRALAM 3850 substrate having a relative permittivity, $\varepsilon_r = 2.9$. The thickness of the antenna metallic (Copper) patch is 18μm while the height of the substrate is 0.1 mm. The loss tangent of Ultralam 3850 laminate is $\tan\delta = 0.0025$. According to the material datasheet supplied by the manufacturer Rogers Corporation, the material parameters of the specified substrate are given at 10 GHz [14]. In order to account for the high-frequency applications, the CST MW studio performs a material characterization for both the dielectric constant and the loss tangent. It generates the corresponding dispersion curves (up to 100 GHz) for both properties using the 2nd order Debye model. The simulated dispersion curves provide quite stable material properties for the entire frequency band under consideration, which further ascertains its stability claimed in the datasheet [14]. In [38], Seiler provided an experimental characterization of Ultralam 3850 for the frequency band of 0.1-67 GHz, while Thompson *et al.* performed such a characterization from the 30-110 GHz band [39]. The results from both analyses indicate that the dielectric properties of the specified laminate are indeed quite stable for the entire bandwidth. For example, in the transmission line (TL) method-based measurement, the loss tangent value does not vary by more than 0.002 over the entire 80 GHz band (30-110 GHz) [39]. Such stable measurement results further validate the material characterization obtained from the CST MW studio-based simulation, which is used to design the antenna proposed in this paper.

The Ultralam 3850 flexible laminate is chosen because of its excellent high-frequency properties and its capability in withstanding the variation of frequency and temperature. The ULTRALAM 3850 is quite a thin material, and hence it has the characteristics of easy bending for flexible and conformal applications, which enables the antenna to be used as a textile antenna. The substrate on which the antenna is mounted has a dimension of 60×40 mm^2. The circular disc-based antenna patch has a radius of 14 mm, and a 50-ohm feed line is used to excite this patch.

Perturbations in the patch and ground plane are instrumental in enhancing the bandwidth of an antenna. Hence, a square slot with a dimension of 4×4 mm^2 is inserted at the center of the circular patch, which is added to a long rectangular notch of 12.13×2 mm^2. The antenna has a partial ground plane with a length of 30.85 mm. A thin rectangular slit of 3.15×0.2 mm^2 is also incorporated into this ground plane, which essentially augments the total bandwidth of the antenna [41], [42].

The proposed antenna has its first resonance (f_1) at 1.74 GHz (as per simulation). For a circular disc monopole antenna, the diameter (D) of the disc plays a crucial role in determining the fundamental mode or first resonance frequency. At this frequency, D roughly equates to the corresponding quarter wavelength [43].

For a given disc radius, R and wavelength, λ_1 at the fundamental mode, the mathematical relationship can be provided by:

$$D = 2R \approx \frac{\lambda_1}{4} \quad (1)\ [43]$$

For relative permittivity, ε_r and velocity of light, $C = 3 \times 10^8$ ms^{-1}, the corresponding wavelength at a given frequency, f can be calculated using the following equation:

$$\lambda = \frac{C}{f\sqrt{\varepsilon_r}} \quad (2)$$

Hence, given the substrate (Ultralam 3850) relative permittivity, $\varepsilon_r = 2.9$, the corresponding wavelength (λ_1) at the fundamental frequency (1.74 GHz) of the proposed antenna is determined as 101.24 mm. Consequently, the corresponding quarter wavelength would be 25.31 mm. The circular disc radius (R) of 14 mm, in turn, indicates that the diameter (D) of

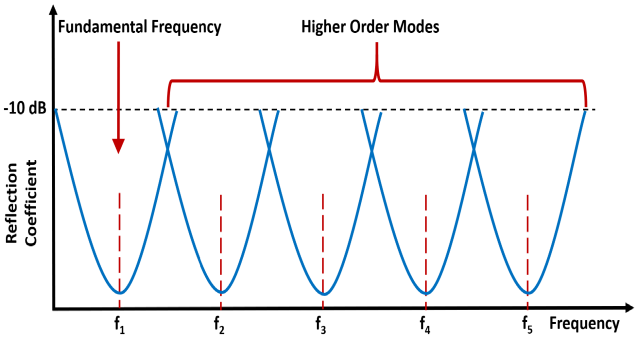

FIGURE 2. Overlapping of adjacent resonances to form SWB [40].

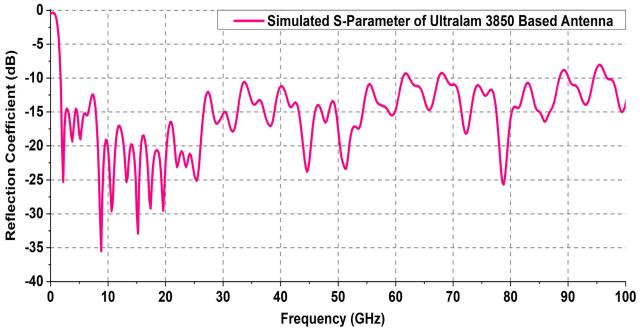

FIGURE 3. Simulated S-parameter of designed antenna.

the disc has a value (28 mm) in the order of the quarter wavelength at antenna fundamental mode. The monopole antenna with circular disc can support numerous resonance modes. The introduced slots and notches on the patch and the ground plane also result in additional harmonics [41], [42]. As mentioned earlier, the first resonance of the antenna is obtained by using the disc dimensions. Thereafter, the subsequent harmonics can be easily determined; since, in essence, they are the higher-order resonances of the fundamental frequency. The operating mechanism of the proposed SWB antenna is shown in Fig. 2. Here, the neighboring resonances involving the fundamental and higher-order modes overlap with each other. This overlap of numerous harmonics closely spaced across the entire spectrum facilitates the antenna to attain super-wide bandwidth [40], [43].

IV. ANALYSIS OF SIMULATED RESULTS

This section analyzes the simulated results of the designed SWB antenna. It provides a comprehensive analysis of the reflection coefficient and far-field patterns, as well as the gain, efficiency, and surface current of the antenna. Fig. 3 exhibits the simulated reflection coefficient of the antenna on Ultralam 3850 substrate. An extensive parametric study has been conducted on the design in order to provide an optimized antenna performance. Fig. 3 illustrates that the proposed antenna covers a frequency band larger than 98 GHz with a bandwidth ratio of 57.47:1. The SWB antenna has an operating range from 1.74 to 100 GHz, with quite a reasonable impedance matching all over the spectrum. Nonetheless, the performance tends to deteriorate slightly at frequencies near 100 GHz. It can be seen that the reflection coefficient reaches a maximum value of -8.05 dB at around 95 GHz; however, the antenna is still functional at such reflection coefficient values. Fig. 4 shows the simulated 3D radiation patterns of the designed antenna. The far-field patterns over a range of frequencies exhibit that the antenna has an omnidirectional pattern at lower bands such as 2 GHz and 5 GHz. However, at higher bands, the radiated power is distributed on top and both sides of the antenna. Interestingly, the radiated power is suppressed in the front and back of the antenna, which indicates low radiation in those areas. This results in the antenna incurring a deviated omnidirectional pattern.

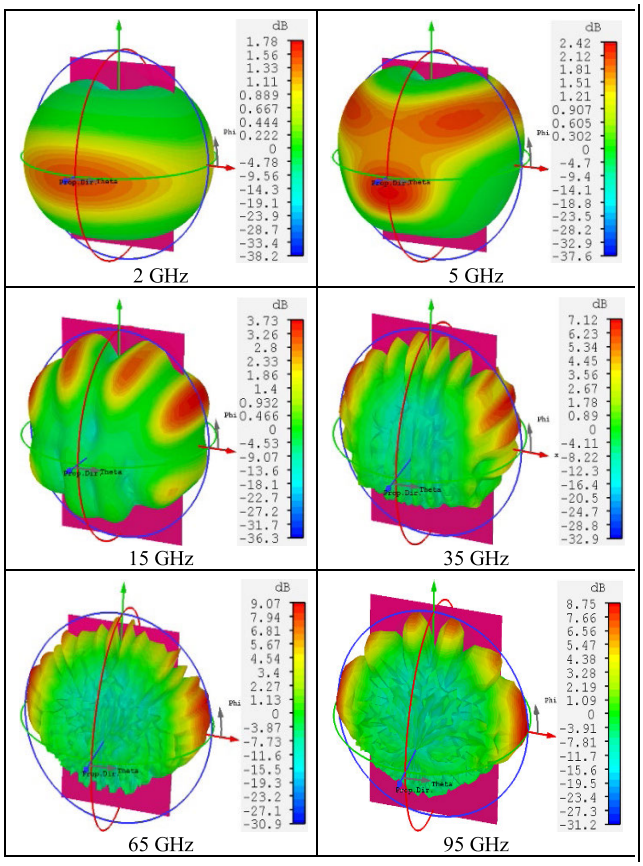

FIGURE 4. Simulated 3D far-field pattern of proposed antenna.

The key mechanism for antenna radiation is the acceleration of charges or variable currents. To facilitate the current variation over an extensive bandwidth, at higher frequencies, the designed circular monopole antenna operates in a hybrid mode of standing and travelling waves [43], [44]. Fig. 5 shows the surface current distribution of the proposed antenna at different frequencies starting from 2-95 GHz. Since the antenna far-field pattern is dependent on surface current [45], this current distribution can be used to explain the antenna radiation mechanism. The overlapping of an increased number of resonance modes of the SWB antenna can be visualized from a number of higher-order modes in the surface current distribution along with a harmonic order flow

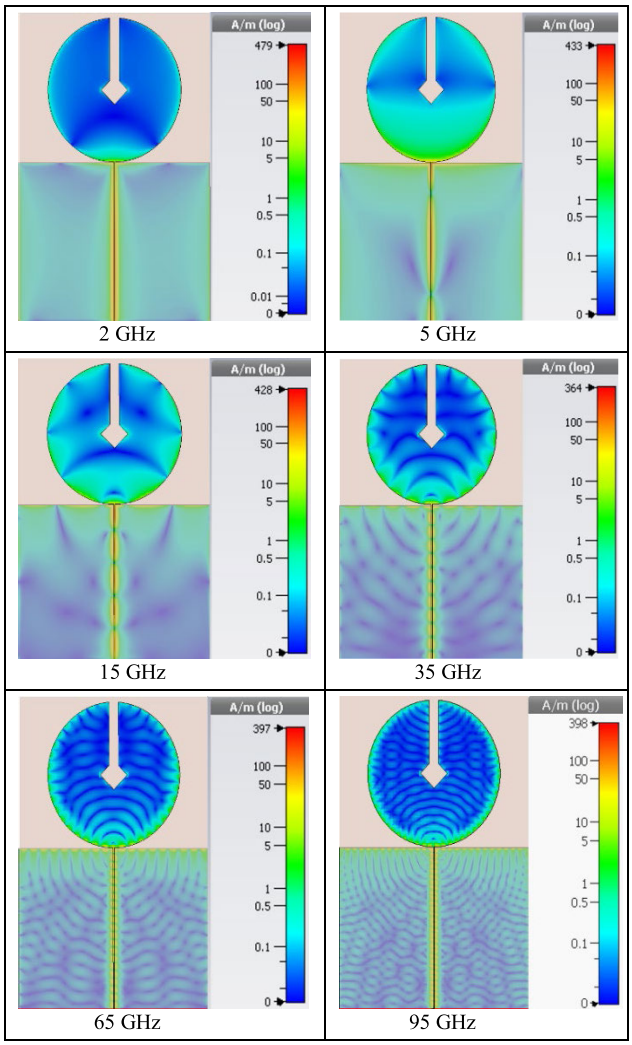

FIGURE 5. Surface current distribution of designed antenna at different frequencies indicating varied resonance modes.

in the feed line, circular disc patch, and the partial ground. Fig. 5 indicates a relatively higher amount of current in the feed line, and therefore, it helps to get a better insight into mode variation. At the lowest operating frequency (2 GHz) under consideration, the first-order harmonic resonance (fundamental mode) is observed. Here, the current mostly propagates along the edges and the lower middle portion of the radiating patch (disc). This generates a standing wave (no net current propagation) with a large envelope hump, which is evident from Fig. 5. The standing wave also surrounds the disc slots, which ensures a current null around them. As a result, the corresponding far-field pattern depicted in Fig. 4 exhibits a donut shape having no radiation from the antenna top [40], [43].

Due to the presence of a comparatively higher current concentration on the lower portion of the disc, the radiated power mostly gets confined to the front side of the antenna. As the frequency increases, the higher-order modes kick in, which can be seen from the current distribution of 5 GHz. At this frequency, the second-order harmonic can be observed. Here, the current propagation mainly takes place in the lower half of the disc. A considerable amount of current also propagates at the top two angular edges of the circular patch, as shown in Fig. 5. Such propagation results in a triangular shape standing wave around the perturbing slots of the disc. Due to such a standing wave, the antenna top incurs a radiating null which resembles the case of 2 GHz. Hence, the antenna radiation pattern still exhibits a donut shape with most radiated power directed towards the antenna front and around the top two angular directions, namely 45° and 135° [40], [43]. The far-field pattern at 15 GHz shows a deformed shape compared to those of 2 GHz and 5 GHz. In this case, an increased number of resonating modes appear, and the current distribution creates a star-shaped standing wave on the antenna surface. The antenna exhibits radiating nulls at the areas that correspond to the vertices of the star shape. The scattered current distribution surrounding the standing wave causes the antenna to radiate mostly in the directions corresponding to those of the surface current. The above analysis illustrates that at lower frequency ranges such as 2-15 GHz, the radiation of the antenna is mostly dominated by the standing wave [40], [43].

At higher frequencies such as 35 GHz, the harmonic orders also increase, which results in a complex surface current distribution on the antenna structure. Owing to such distribution, the circular patch operates on a hybrid mode that combines both the standing and travelling waves. In this case, the travelling wave plays a dominant role. However, as shown in Fig. 5, a standing wave is also formed around the perturbing slots and on the circular disc surface. As a result, the current mostly propagates across a range of scattered areas on the disc edge, and the disc surface suffers from a significant amount of current null. This provides an inference into the deformation of the radiation pattern at such frequencies, as shown in Fig. 4 [40], [43]. Here, the radiated power gets suppressed in the front and back of the patch, and mostly the corresponding radiating patch edges contribute to the formation of the far-field radiation resulting in a deviated omnidirectional pattern. The far-field patterns at 65-95 GHz also exhibit a similar trend. The higher the frequency goes, the more the number of harmonic order increases. Such increment eventually reaches an extent where the resonating modes start to overlap with each other. The hybrid mode of operation prompts the antenna circular disc patch to confine the current concentration across its edges. This results in the antenna radiating from the patch edges, which is similar to the case of 35 GHz. However, the increasingly dense distribution of standing and travelling waves over the entire circular patch makes the propagation of current-carrying waves quite challenging. As a result, the far-field patterns at these frequencies incur extreme deformation, and therefore, are shaped to become highly asymmetric, which is evident from Fig. 4 [43], [46]. The presence of both of the standing and travelling waves at higher frequency ranges ensure that the net current propagation around the perturbing slots of the disc is not always zero. In contrast to the lower frequency bands, here, the hybrid mode allows a

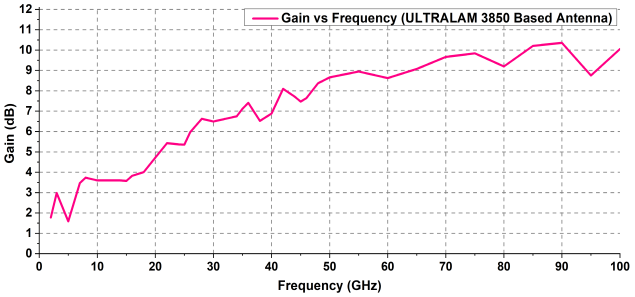

FIGURE 6. Simulated maximum gain vs frequency of designed antenna.

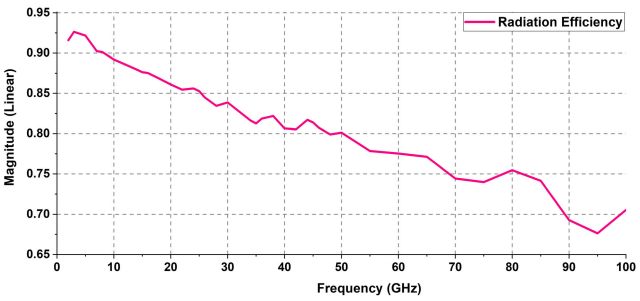

FIGURE 7. Simulated radiation efficiency plot of the designed antenna.

considerable proportion of current to propagate around the slots. As a result, the antenna radiates a significant amount of power to the upward direction, which is essentially the effect of the radio energy propagation from the specified slot region.

The simulation result for maximum gain vs. frequency is depicted in Fig. 6. Barring some fluctuations, this plot indicates an upward trend of gain values with increasing frequency. The gain magnitude is relatively lower in the lower range of frequencies; however, as the frequency increases, gain also assumes higher values. The maximum gain value of 10.35 dB is recorded at 90 GHz. Fig. 7 shows the simulated radiation efficiency plot of the antenna on the Ultralam 3850 laminate. It can be seen that the antenna efficiency decreases gradually with increasing frequency. Apart from the loss that occurs from impedance mismatch, the designed antenna incurs some ohmic or real power loss.

Ohmic loss typically occurs due to the finite conductivity of the metal (copper) used in the antenna. This loss is more prominent in the case of small or miniaturized antennas [47]. The total ohmic loss of an antenna is the one that dissipates in the antenna loss resistance (R_L). The antenna efficiency is a function of radiation resistance (R_r) and loss resistance (R_L) given by equation (3):

$$\text{Efficiency} = \frac{R_r}{R_r + R_L} \tag{3}$$

The radiation resistance is a function of antenna wavelength. Antennas typically exhibit high radiation resistance if the wavelength is high. This, in turn, increases the antenna efficiency. However, at higher frequencies, the corresponding wavelengths of the proposed antenna become smaller, which causes a reduction in its radiation resistance [48]. This reduction in radiation resistance results in lower efficiency of the antenna at higher frequencies. The linear scale plot depicted in Fig. 7 illustrates that based on the operating frequency, the radiation efficiency approximately ranges from a maximum of 93% to a minimum of 67.6%. From 1.74 to 90 GHz, the antenna offers an efficiency of at least 70%. A slight fluctuation is observed at higher bands, which eventually reaches down to 67.6% at 90 GHz before offering back 70% efficiency at 100 GHz. This indicates that the designed antenna is a pretty efficient radiator since it provides more than 65% efficiency even at such high frequencies.

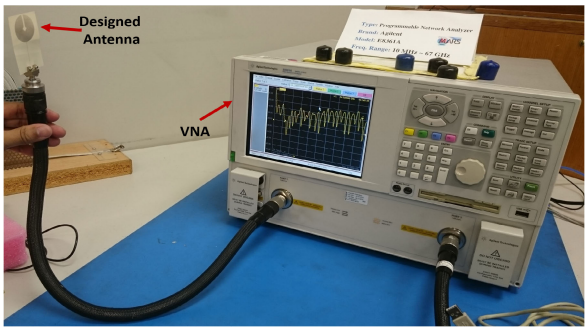

FIGURE 8. Measurement set-up for reflection coefficient calculation of fabricated antenna.

V. ANALYSIS OF MEASURED RESULTS

A laboratory prototype of the proposed antenna is developed and experimentally tested using the Keysight E8361A programmable network analyzer (PNA). The E8361A covers an operating range of up to 67 GHz. Hence, the experimental measurement of the antenna prototype is performed only up to this frequency band. To ensure a seamless measurement, the antenna is connected to the PNA using the 1892-04A-5 End Launch connector from the southwest microwave. This connector also has an operating range of up to 67 GHz. Fig. 8 and Fig. 9 represent the experimental set-up and the measured reflection coefficient vs. frequency plot for the designed antenna. Fig. 9 shows the reflection coefficient vs. frequency plot for the Ultralam 3850 laminate-based flexible antenna. The specified plot reveals that the antenna has a very good impedance matching with a reflection coefficient below-10 dB in the entire operating band from 1.96 to 67 GHz. This indicates that the antenna a bandwidth larger than 65 GHz with a ratio bandwidth of 34.18:1. The offset frequency lower limit of this antenna from its simulated counterpart (1.74 GHz) is 220 MHz.

Fig. 10 shows the comparative plots of simulated and measured elevation (E-plane) and azimuth (H-plane) far-field patterns for the designed antenna. The experimental measurement of the far-field pattern is carried out in an anechoic chamber. To account for the far-field distance at the maximum operating band (67 GHz), the designed antenna and another of its identical counterpart are positioned at a distance of 35 cm apart from each other. The figures depict that at 5 GHz, the antenna has an omnidirectional far-field

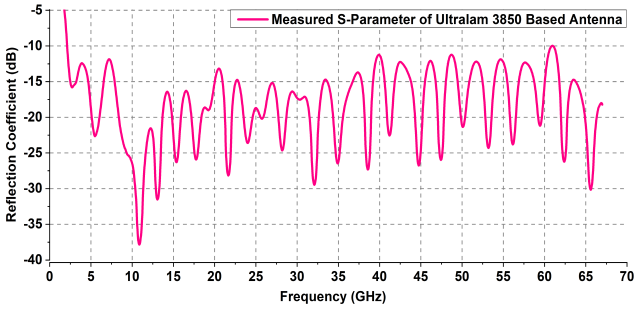

FIGURE 9. Measured S-parameter of fabricated antenna.

pattern. At 20 GHz, the pattern incurs a slight distortion from that of the 5 GHz case; however, as the frequency of interest goes further up, a significant pattern deformation with an increased number of ripples becomes evident. It can also be observed that the radiation pattern at 5 GHz has a typical figure of eight shape. As compared to the 3D pattern depicted in Fig. 4, the polar plot also represents the fact that the antenna radiated power is distributed to the top and both the sides of the radiator at increased frequencies.

As the frequency increases further, the number of ripples also get increased due to higher-order modes. This is essentially the effect of the complex surface current distribution at higher-order harmonics and the resulting hybrid mode of operation in the circular patch antenna, which is illustrated in section IV. Due to the presence of such ripples, at higher bands, the proposed antenna deviates from its omnidirectional radiation characteristics. The radiating null at some directions indicates that the antenna may not be the best choice for applications that require absolutely omnidirectional radiation. For example, it will not be a good choice to deploy in moving vehicles, where the ability to radiate uniformly in all directions is quite essential. Similarly, it may not offer the best solution for applications using high-frequency portable devices. However, the ability of the antenna to radiate more in some specified directions makes it a better-suited choice for 5G applications.

The comparative plots of simulated and measured gain vs. frequency at broadside direction shown in Fig. 11 indicate that they typically follow a similar trend portrayed by the simulated maximum gain results in Fig. 6. The measured gain is obtained by employing the absolute gain method, which makes use of the standard Friis transmission formula [49]. Similar to the simulated gain, the experimental gain also exhibits a trend of having low amplitude at lower bands. With increasing frequency bands, the amplitude of the gain generally tends to have comparatively higher values, although a substantial fluctuation is quite apparent. The designed antenna exhibits a peak gain of 9.24 dB at 65.6 GHz. It can be seen that the antenna exhibits a gain value of lower than 0 dB at a certain number of frequency bands. The main reason for incurring such a low gain is the direction in which

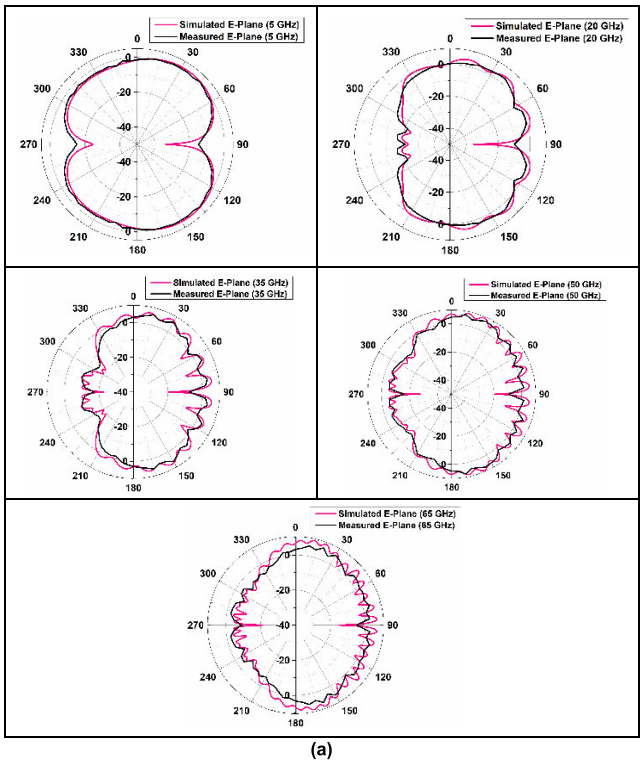

(a)

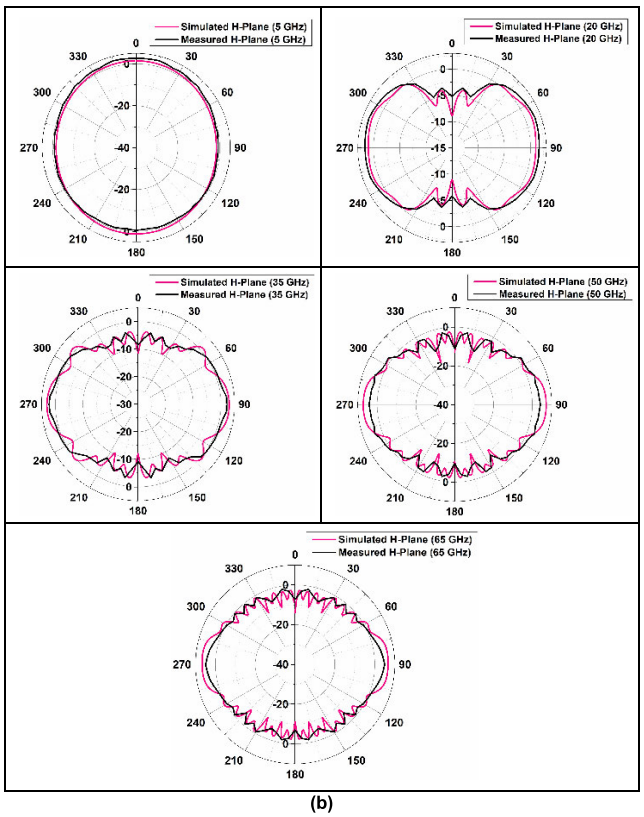

(b)

FIGURE 10. Far-field pattern of fabricated antenna (a) E-Plane (b) H-Plane.

the gain measurement is performed. As depicted in Fig. 4, the proposed antenna has an omnidirectional far-field pattern at lower frequency bands, which gets deviated at higher

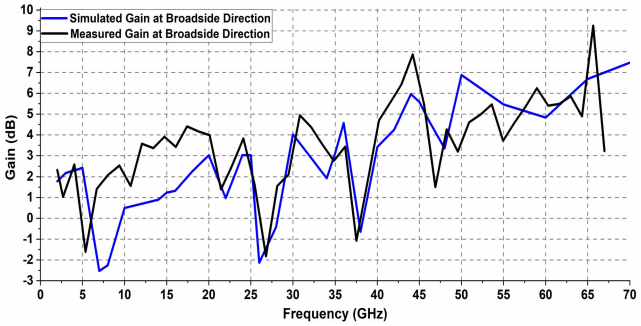

FIGURE 11. Comparative plots of simulated and measured gain at broadside direction.

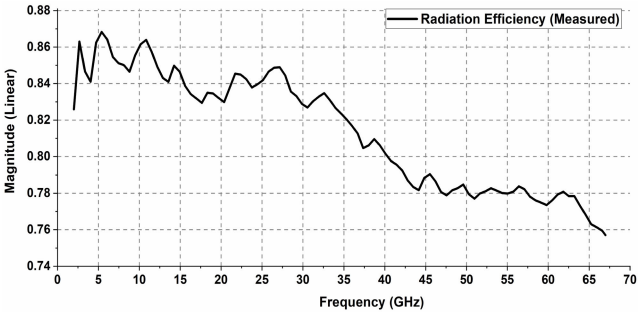

FIGURE 12. Measured radiation efficiency plot of the designed antenna.

ranges. This indicates that the antenna changes the direction of its maximum radiation based on frequencies.

For example, at frequencies around 15 GHz or higher, the antenna mainly radiates from the circular disc (patch) edges, making the radiation confined mostly towards the end-fire direction while a comparatively smaller amount of power is still radiated in broadside. Owing to such characteristics, at some frequency bands, the broadside radiation of the antenna remains extremely poor. However, the gain of this antenna is experimentally measured in the broadside direction only. Hence, the experimental gain at those specified frequency bands exhibits considerably lower values. Nevertheless, even though the measured gain in the broadside direction is low, the other directions often have a high radiated power at the same corresponding frequencies. This bestows the fact that the antenna is quite effective even at frequencies where the measured gain is lower than 0 dB. The simulated gain depicted in Fig. 6 shows the maximum gain irrespective of directions, while both of the simulated and measured gain plots portrayed in Fig. 11 exhibit the gain for broadside only.

The efficiency of the antenna is measured using the Wheeler Cap method. The measured antenna efficiency plot is shown in VII. Although the measured plot is similar to its simulated counterpart depicted in Fig. 7, a bit of discrepancy can still be observed. This occurs due to the difference in ohmic and impedance mismatch loss. The measurement is carried out in an open lab (not in an anechoic chamber) environment, which also affected the results due to EM noise. It can be seen that, depending on frequencies, the measured

TABLE 1. Front to back ratio at different frequencies.

Frequency	Front to Back Ratio	
	Linear	dB
2 GHz	1	0
15 GHz	2.84	4.54
35 GHz	7.78	8.91
65 GHz	10.78	10.33

TABLE 2. Bandwidth (BW) comparison with selected SWB antennas reported in literature.

Ref.	Design	Size (mm^3)	Impedance BW (GHz)	Ratio BW
[10]	Measured	35×77×1.6	1.44-18.8	13.06:1
[11, 17]	Simulated	16.55×15.72 ×0.787	5-150	30:1
	Measured		5-50	10:1
[18]	Simulated	31×45×1.575	2.18-44.5	20.4:1
	Measured		2-18-20	9.17
[19]	Simulated	24×18×0.787	11-200	18.18:1
[23]	Simulated	30×40×0.787	0.9-100	111.1:1
	Measured		0.9-25	27.77
[28]	Simulated	57×34×1	1.42-90	63.38:1
	Measured		1.42-50	35.21:1
[50]	Measured		0.72-25	34.72:1
[51]	Simulated	28×27×1.6	2.75-71	25.82:1
	Measured		2.75-50	18.18:1
[52]	Simulated	40×30×1.6	2.5-80	32:1
	Measured		2-25	12.5:1
Proposed	Simulated	60×40×0.1	1.74-100	57.47:1
	Measured		1.96-67	34.18:1

antenna efficiency varies between 75.7%-86.8%. Although the measured gain of the antenna exhibits negative gain at some frequencies, for the entire measured frequency band of 2-67 GHz, the efficiency never goes below 75%. This indicates that even at those frequencies, the antenna has a positive gain in some other directions.

The frequency-wise evaluated front-to-back (F/B) ratios of the designed antenna are shown in Table 1. As the far-field pattern is mostly omnidirectional at lower bands, the calculated ratio for the antenna is found to be 0 dB at 2 GHz. At higher frequency bands, the far-field pattern tends to become directional, causing a gradual increment of the F/B ratio. Table 2 provides a comparative study of the proposed antenna with the experimentally validated SWB antennas available in the literature.

Taking account of the highest measurement limit (67 GHz), Table 2 depicts a ratio bandwidth of 34.18:1 for the fabricated antenna on Ultralam 3850 laminate. Amongst all the reported experimentally tested wideband antennas in the literature, the proposed antenna has the maximum measured frequency range, and it provides one of the highest achieved bandwidth ratios.

VI. APPLICABILITY IN 5G

One of the prime specifications or features of the fifth-generation (5G) technology is the enhanced Mobile Broadband (eMBB). Deployment of eMBB will enable the 5G network to offer an increased data rate, capacity, and

coverage over its preceding generations. eMBB is essentially an extended version of the 4G broadband service [53]. Such evolution of mobile broadband is ensured by adopting a unified and more capable radio interface termed as 5G New Radio (NR). Along with the existing frequency spectrum of 4G LTE, the 5G NR global standard has specified certain frequency ranges in the mmWave bands (26, 28, 40, 59, and 66 GHz) [2]. However, to provide ubiquitous connectivity for a wide range of applications, this standard will enable the adoption of an adaptive bandwidth with a high degree of spectrum flexibility [54]. Therefore, the 5G communication system needs to cater for an extremely high bandwidth starting from below 1 GHz to 100 GHz based on different deployments. This instigates the demand for low-cost and compact antennas that can cover a broad bandwidth. The proposed antenna in this paper covers the entire high-frequency spectrum of the 5G NR global standard while providing a high gain and radiation efficiency. The increased spectrum availability makes the 5G radio technology a key IoT enabler by supporting the high traffic growth and growing demand for high-bandwidth connectivity. IoT performs as a bridge between technology capabilities and business applications. The pervasive coverage, low latency, and high-speed connectivity of 5G allow a substantial number of IoT devices to communicate with each other seamlessly. This eventually enables a wide range of industrial applications to take advantage of such a groundbreaking technology. For example, 5G is poised to play a significant role in driving industrial automation. It will also support the use cases like smart homes, precision agriculture, transport infrastructures such as connected cars and traffic control, health monitoring of public infrastructures such as bridges, wearables, and many others [54]. Due to the wide operating band of the proposed antenna, it can be used as an integral part of the transceiver interface in such applications. The flexibility and conformal characteristics of the antenna allow it to be used for WBAN applications as well. This antenna can be deployed in the on-body environment along with the physiological sensors that constantly monitor the vital signs of a person. The integration of the proposed antenna can ensure the transmission of such data to a server. Thus it enables a continuous remote health monitoring of patients in an ambulatory setting for abnormality detection as well as supervised rehabilitation [55]. In addition to the currently used macro cell-based radio access network, 5G will deploy the small cells. These cells are portable miniature base stations that use less power to operate in a typical coverage area of 50-250 meters. The antennas at these cells are required to transmit mmWave signals, and therefore, the size of these antennas can be much smaller than the traditional antennas used in macro cells. In this regard, the proposed SWB antenna can be considered a very good candidate since it has a compact dimension along with the operability at mmWave bands [56]. To achieve a greater network capacity, 5G will make use of the Massive MIMO technology. This technology equips the base stations (5G macro cells) with arrays of a very large number of antennas and thereby forms the advanced antenna systems (AAS). AAS enables simultaneous transmission of data to multiple users using the same time-frequency resource through separate beams [57]. The compact size of the proposed antenna makes it a well-suited choice for AAS. The deviated omnidirectional radiation pattern with directive beams in multiple directions also bestows its tremendous potential as a 5G antenna. Such radiation characteristics will ensure more directive beams with an enhanced gain when an array is implemented based on the proposed antenna. However, the design of the antenna array is out of the scope of this paper.

VII. CONCLUSION

This article illustrates the design and experimental analysis of a compact SWB antenna. The antenna is designed on a thin and flexible Ultralam 3850 laminate. This electrically small antenna has a physical dimension of $60\times40\times0.1$ mm^3, and it uses a circular disc monopole structure to cover a ratio bandwidth of 57.47:1. Here, the simulated performance of the designed antenna is thoroughly analyzed in terms of its reflection coefficient, radiation pattern, gain, radiation efficiency, and surface current. The far-field behavior of the SWB antenna at different frequencies is theoretically explained from the antenna's surface current analysis. A laboratory prototype of the proposed antenna is manufactured, and the experimental verification reveals excellent consistency between the simulation and measurement results. Due to hardware limitations, the antenna is measured up to 67 GHz, which gives an impedance bandwidth from 1.96 to 67 GHz with a bandwidth ratio of 34.18:1. By far, this is one of the highest achieved ratio bandwidths among the practically fabricated and measured wideband antennas reported in the literature. By increasing the patch thickness, the enclosed spherical volume of this antenna can be utilized effectively. This enhances the bandwidth further by improving volumetric antenna efficiency [21]. An experimental research to validate the above theoretical concept is currently underway. The proposed antenna operates in a diverse range of application bands, including near field communication (NFC), wireless networking, RFID, ZigBee, GPS, Bluetooth, 4G LTE, Wireless LAN, WiMAX, microwave, and satellite communications. The flexible structure of this antenna allows it to be used for wireless body area network (WBAN) based applications as well. More importantly, the proposed SWB antenna can cover most of the existing and forthcoming 5G application bands, including massive MIMO and mmWave. Considering all the above factors, it can be inferred that the designed antenna is an excellent addition to the antenna research community since it combines its flexible structure with the SWB technology to provide operability in a wide range of exciting applications involving WBAN, 5G, and IoT.

REFERENCES

[1] T. S. Rappaport, Y. Xing, G. R. MacCartney, A. F. Molisch, E. Mellios, and J. Zhang, "Overview of millimeter wave communications for fifth-generation (5G) wireless networks—With a focus on propagation models," *IEEE Trans. Antennas Propag.*, vol. 65, no. 12, pp. 6213–6230, Dec. 2017, doi: 10.1109/TAP.2017.2734243.

[2] L. Camargos. (2019). *WRC-19 Strikes a Good Balance, Sets Stage for mmWave 5G—Spectrum*. Accessed: Oct. 9, 2020. [Online]. Available: https://www.gsma.com/spectrum/wrc-19-strikes-good-balance-sets-stage-for-mmwave-5g/

[3] CableFree. (2019). *5G Frequency Bands & Spectrum Allocations*. Accessed: Jan. 9, 2020. [Online]. Available: https://www.cablefree.net/wirelesstechnology/4glte/5g-frequency-bands-lte/

[4] (2019). *5G Network Uses Nearly Same Frequency as Weaponized Crowd Control Systems RF (Radio Frequency) Safe*. Accessed: Dec. 15, 2019. [Online]. Available: https://www.rfsafe.com/5g-network-uses-nearly-same-frequency-as-weaponized-crowd-control-systems/

[5] U. Rafique, H. Khalil, and R. S. Ur, "Dual-band microstrip patch antenna array for 5G mobile communications," presented at the Prog. Electromagn. Res. Symp., Fall (PIERS, FALL), Nov. 2017.

[6] C. Z. Ning and L. Kwai-Man, "Fundamentals of antennas," in *Antennas for Base Stations in Wireless Communications*. New York, NY, USA: McGraw-Hill, 2009.

[7] A. Alomainy, Y. Hao, and F. Pasveer, "Antennas for wearable devices," in *Antennas for Portable Devices*. Hoboken, NJ, USA: Wiley, 2007, pp. 197–229.

[8] J. L. Volakis, C.-C. Chen, and K. Fujimoto, *Small Antennas: Miniaturization Techniques & Applications*. New York, NY, USA: McGraw-Hill, 2010, pp. 3–100.

[9] R. Bancroft. (2004). *Fundamental Dimension Limits of Antennas Ensuring Proper Antenna Dimensions in Mobile Device Designs*. Accessed: Mar. 5, 2020. [Online]. Available: https://www.semanticscholar.org/paper/Fundamental-Dimension-Limits-of-Antennas-Ensuring-Bancroft/985a19c7e4e851851eb523d7ff6cbb5ba5092988

[10] K.-R. Chen, C.-Y.-D. Sim, and J.-S. Row, "A compact monopole antenna for super wideband applications," *IEEE Antennas Wireless Propag. Lett.*, vol. 10, pp. 488–491, 2011, doi: 10.1109/LAWP.2011.2157071.

[11] D. Tran, "On the design of a super wideband antenna," in *Ultra Wideband*, B. Lembrikov, Ed. London, U.K.: IntechOpen, 2010, ch. 17, pp. 399–426.

[12] S. Mahmud, S. Dey, and N. Saha, "Super wide band wearable antenna: Assessment of the conformal characteristics in terms of impedance matching and radiation properties," in *Proc. IEEE Int. Symp. Antennas Propag. (ISAP)*, Oct./Nov. 2012, pp. 563–566.

[13] J. G. Santas, A. Alomainy, and Y. Hao, "Textile antennas for on-body communications: Techniques and properties," in *Proc. IET Conf.*, 2007, p. 537. [Online]. Available: https://digital-library.theiet.org/content/conferences/10.1049/ic.2007.1064

[14] (2008). *ULTRALAM 3000 Liquid Crystalline Polymer Circuit Material*. Accessed: Nov. 6, 2020. [Online]. Available: http://www.clarke.com.au/pdf/ULTRALAM__3000_LCP_laminate_data_sheet__ULTRALAM_3850.pdf

[15] S. Barbarino and F. Consoli, "Study on super-wideband planar asymmetrical dipole antennas of circular shape," *IEEE Trans. Antennas Propag.*, vol. 58, no. 12, pp. 4074–4078, Dec. 2010, doi: 10.1109/TAP.2010.2078469.

[16] X.-H. Jin, X.-D. Huang, C.-H. Cheng, and L. Zhu, "Super-wideband printed asymmetrical dipole antenna," *Prog. Electromagn. Res. Lett.*, vol. 27, no. 8, pp. 117–123, 2011.

[17] D. Tran, A. Szilagyi, I. E. Lager, P. Aubry, L. P. Ligthart, and A. Yarovoy, "A super wideband antenna," presented at the 5th Eur. Conf. Antennas Propag. (EUCAP), Apr. 2011.

[18] M. A. Dorostkar, M. T. Islam, and R. Azim, "Design of a novel super wide band circular-hexagonal fractal antenna," *Prog. Electromagn. Res.*, vol. 139, no. 7, pp. 229–245, 2013.

[19] H. M. Bernety, B. Zakeri, and R. Gholami, "A compact directional super-wideband antenna," presented at the 21st Iranian Conf. Electr. Eng. (ICEE), May 2013.

[20] J. Liu, K. P. Esselle, S. G. Hay, and S. S. Zhong, "Compact super-wideband asymmetric monopole antenna with dual-branch feed for bandwidth enhancement," *Electron. Lett.*, vol. 49, no. 8, pp. 515–516, Apr. 2013, doi: 10.1049/el.2012.4015.

[21] S. Dey and N. C. Karmakar, "Design of novel super wide band antennas close to the small antenna limitation theory," presented at the IEEE MTT-S Int. Microw. Symp. Dig., Jun. 2014.

[22] M. A. Jamlos, W. A. Mustafa, W. Khairunizam, I. Zunaidi, Z. M. Razlan, and A. B. Shahriman, "Stacked stepped-fed super wideband antenna performance in free space and liquid medium for biomedical applications," *IOP Conf. Ser., Mater. Sci. Eng.*, vol. 557, Jun. 2019, Art. no. 012026, doi: 10.1088/1757-899x/557/1/012026.

[23] M. Manohar, R. S. Kshetrimayum, and A. K. Gogoi, "Super wideband antenna with single band suppression," *Int. J. Microw. Wireless Technol.*, vol. 9, no. 1, pp. 143–150, Feb. 2017, doi: 10.1017/S1759078715000963.

[24] J. Liu, K. P. Esselle, S. G. Hay, Z. Sun, and S. Zhong, "A compact super-wideband antenna pair with polarization diversity," *IEEE Antennas Wireless Propag. Lett.*, vol. 12, pp. 1472–1475, 2013, doi: 10.1109/LAWP.2013.2287500.

[25] R. Jinger and N. Agrawal, "Design and development of compact super-wideband antenna with integrated Bluetooth band," presented at the Int. Conf. Adv. Comput. Netw. Inform., Singapore, 2019.

[26] S. Singhal, J. Budania, and A. K. Singh, "Elliptical monopole based super wideband fractal antenna," *Microw. Opt. Technol. Lett.*, vol. 62, no. 3, pp. 1324–1328, Mar. 2020, doi: 10.1002/mop.32143.

[27] S. Singhal, "Asymmetrically fed octagonal Sierpinski band-notched super-wideband antenna," *J. Comput. Electron.*, vol. 16, no. 1, pp. 210–219, Mar. 2017, doi: 10.1007/s10825-016-0948-5.

[28] S. U. Rahman, Q. Cao, H. Ullah, and H. Khalil, "Compact design of trapezoid shape monopole antenna for SWB application," *Microw. Opt. Technol. Lett.*, vol. 61, no. 8, pp. 1931–1937, Aug. 2019, doi: 10.1002/mop.31805.

[29] M. Alibakhshikenari, B. S. Virdee, C. H. See, R. A. Abd-Alhameed, F. Falcone, and E. Limiti, "Super-wide impedance bandwidth planar antenna for microwave and millimeter-wave applications," *Sensors*, vol. 19, no. 10, p. 2306, May 2019, doi: 10.3390/s19102306.

[30] M. N. Rahman, M. T. Islam, M. Z. Mahmud, and M. Samsuzzaman, "Compact microstrip patch antenna proclaiming super wideband characteristics," *Microw. Opt. Technol. Lett.*, vol. 59, no. 10, pp. 2563–2570, Oct. 2017, doi: 10.1002/mop.30770.

[31] D. Q. Liu, H. J. Luo, M. Zhang, H. L. Wen, B. Wang, and J. Wang, "An extremely low-profile wideband MIMO antenna for 5G smartphones," *IEEE Trans. Antennas Propag.*, vol. 67, no. 9, pp. 5772–5780, Sep. 2019, doi: 10.1109/TAP.2019.2908261.

[32] M. S. Mahmud and S. Dey, "Design and performance analysis of a compact and conformal super wide band textile antenna for wearable body area applications," presented at 6th Eur. Conf. Antennas Propag. (EUCAP), Mar. 2012.

[33] S. Dey and N. C. Karmakar, "Design of novel super wide band antenna close to the fundamental dimension limit theory," *Sci. Rep.*, vol. 10, no. 1, p. 16306, Dec. 2020, doi: 10.1038/s41598-020-73478-2.

[34] W. Balani, M. Sarvagya, T. Ali, M. Pai M. M., J. Anguera, A. Andujar, and S. Das, "Design techniques of super-wideband antenna–existing and future prospective," *IEEE Access*, vol. 7, pp. 141241–141257, 2019, doi: 10.1109/ACCESS.2019.2943655.

[35] Wikipedia Free Encyclopedia. (Dec. 24, 2014). *Q Band*. [Online]. Available: https://en.wikipedia.org/w/index.php?title=Q_band&oldid=639478523

[36] W. Haiming, H. Wei, C. Jixin, S. Bo, and P. Xiaoming, "IEEE 802.11aj (45 GHz): A new very high throughput millimeter-wave WLAN system," *China Commun.*, vol. 11, no. 6, pp. 51–62, Jun. 2014, doi: 10.1109/CC.2014.6879003.

[37] *IEEE Standard for Information Technology–Telecommunications and Information Exchange Between Systems Local and Metropolitan Area Networks–Specific Requirements Part 11: Wireless LAN Medium Access Control (MAC) and Physical Layer (PHY) Specifications Amendment 3: Enhancements for Very High Throughput to Support Chinese Millimeter Wave Frequency Bands (60 GHz and 45 GHz)*, IEEE Standard 802.11aj-2018, (Amendment to IEEE Standard 802.11-2016 as amended by IEEE Standard 802.11ai-2016 and IEEE Standard 802.11ah-2016), 2018, pp. 1–306, doi: 10.1109/IEEESTD.2018.8345727.

[38] P. Seiler, "Dielectric material characterization up to terahertz frequencies using planar transmission lines," Ph.D. dissertation, Dept. Electr. Comput. Eng., Tech. Univ. Dresden, Dresden, Germany, 2019.

[39] D. C. Thompson, O. Tantot, H. Jallageas, G. E. Ponchak, M. M. Tentzeris, and J. Papapolymerou, "Characterization of liquid crystal polymer (LCP) material and transmission lines on LCP substrates from 30 to 110 GHz," *IEEE Trans. Microw. Theory Techn.*, vol. 52, no. 4, pp. 1343–1352, Apr. 2004, doi: 10.1109/TMTT.2004.825738.

[40] S. Preradovic, "Chipless RFID system for barcode replacement," Ph.D. dissertation, Dept. Electr., Comput. Syst. Eng., Monash Univ., Melbourne, VIC, Australia, 2009.

[41] S. A. R. Parizi, "Bandwidth enhancement techniques," in *Trends in Research on Microstrip Antennas*, S. Chattopadhyay, Ed. Rijeka, Croatia: InTech, 2017, pp. 3–37.

[42] M. Huynh, "Wideband compact antennas for wireless communication applications," Ph.D. dissertation, Dept. Electr. Comput. Eng., Virginia Polytech. Inst. State Univ., Blacksburg, VA, USA, 2004.
[43] X. Chen and P. J. Massey, "Operating principles and features of UWB monopoles and dipoles," presented at the IET Seminar Ultra Wideband Syst., Technol. Appl., Apr. 2006.
[44] W. Wiesbeck, G. Adamiuk, and C. Sturm, "Basic properties and design principles of UWB antennas," *Proc. IEEE*, vol. 97, no. 2, pp. 372–385, Feb. 2009.
[45] S. Noghanian and L. Shafai, "Control of microstrip antenna radiation characteristics by ground plane size and shape," *IEE Proc., Microw., Antennas Propag.*, vol. 145, no. 3, pp. 207–212, 1998, doi: 10.1049/ip-map:19981819.
[46] N. Behdad and K. Sarabandi, "A compact antenna for ultrawideband applications," *IEEE Trans. Antennas Propag.*, vol. 53, no. 7, pp. 2185–2192, Jul. 2005, doi: 10.1109/TAP.2005.850750.
[47] S. I. Latif, L. Shafai, and C. Shafai, "Gain and efficiency enhancement of compact and miniaturised microstrip antennas using multi-layered laminated conductors," *IET Microw., Antennas Propag.*, vol. 5, no. 4, pp. 402–411, 2011, doi: 10.1049/iet-map.2010.0061.
[48] S. Gibilisco, *Teach Yourself Electricity and Electronics*, 6th ed. New York, NY, USA: McGraw-Hill, 2016.
[49] *IEEE Standard Test Procedures for Antennas*, ANSI/IEEE Standard 149-1979, 1979, p. 1, doi: 10.1109/IEEESTD.1979.120310.
[50] J. Liu, K. P. Esselle, S. G. Hay, and S.-S. Zhong, "Study of an extremely wideband monopole antenna with triple band-notched charactersistics," *Prog. Electromagn. Res.*, vol. 123, no. 2, pp. 143–158, 2012.
[51] S. Singhal and A. K. Singh, "Asymmetrically CPW-fed circle inscribed hexagonal super wideband fractal antenna," *Microw. Opt. Technol. Lett.*, vol. 58, no. 12, pp. 2794–2799, Dec. 2016, doi: 10.1002/mop.30156.
[52] M. Manohar, R. S. Kshetrimayum, and A. K. Gogoi, "Printed monopole antenna with tapered feed line, feed region and patch for super wideband applications," *IET Microw., Antennas Propag.*, vol. 8, no. 1, pp. 39–45, Jan. 2014, doi: 10.1049/iet-map.2013.0094.
[53] O. Teyeb, G. Wikström, M. Stattin, T. Cheng, S. Faxér, and H. Do. (2017). Evolving LTE to fit the 5G future. Ericsson Technology Review. Accessed: Nov. 3, 2020. [Online]. Available: https://www.ericsson.com/en/reports-and-papers/ericsson-technology-review/articles/evolving-lte-to-fit-the-5g-future
[54] E. Dahlman, G. Mildh, S. Parkvall, J. Peisa, J. Sachs, and Y. Selen. (2014). *5G Radio Access*. Accessed: Nov. 5, 2020. [Online]. Available: https://www.ericsson.com/en/reports-and-papers/ericsson-technology-review/articles/5g-radio-access
[55] R. W. Jones and K. Katzis, "5G and wireless body area networks," presented at IEEE Wireless Commun. Netw. Conf. Workshops (WCNCW), Apr. 2018.
[56] A. Nordrum and K. Clark. (2017). *Everything You Need to Know About 5G IEEE Spectrum: Technology, Engineering, and Science News*. Accessed: Nov. 10, 2020. [Online]. Available: https://spectrum.ieee.org/video/telecom/wireless/everything-you-need-to-know-about-5g
[57] P. Butovitsch, D. Astely, C. Friberg, A. Furuskär, B. Göransson, B. Hogan, J. Karlsson, and E. Larsson. (2018). *Advanced Antenna Systems for 5G Networks*. Accessed: Nov. 5, 2020. [Online]. Available: https://www.ericsson.com/en/reports-and-papers/white-papers/advanced-antenna-systems-for-5g-networks

SHUVASHIS DEY (Member, IEEE) received the Bachelor of Technology (B. Tech) degree in electronics and communication engineering from the National Institute of Technology, Durgapur, West Bengal, India, in 2007, the M.Sc. degree in wireless networks (physical pathway) from the Queen Mary University of London, England, U.K., in 2009, and the Ph.D. degree in electrical and computer systems engineering from Monash University, Australia, in 2018.

He is a Postdoctoral Research Fellow with the Department of Electrical and Computer Systems Engineering, Monash University. Since 2016, he has been a Research Affiliate with the Auto-ID Laboratory, Massachusetts Institute of Technology (MIT), Cambridge, USA. From 2010 to 2013, he was a Lecturer with the American International University-Bangladesh (AIUB), Dhaka, Bangladesh. His research interests include the microwave devices and antennas, wearable antennas for healthcare applications, and chipless and chip-based UHF RFID tag and sensors.

Mr. Dey's awards and honors include the Young Scientist's Travel Grant at 2012 IEEE International Symposium on Antennas and Propagation (ISAP), the IEEE MTT-S Ph.D. Student Sponsorship Initiative Award, in 2016, and the Best Presentation Award at 2017 International Conference on Sensing Technology (ICST).

MD SHAMSUL AREFIN received the B.S. degree in electrical and electronics engineering from the Bangladesh University of Engineering and Technology (BUET), Dhaka, Bangladesh, in 2007, the M.S. degree in electrical engineering from Northern Arizona University, Flagstaff, AZ, USA, in 2010, and the Ph.D. degree in electronic engineering from Monash University, Melbourne, Australia, in 2017.

From February 2017 to February 2018, he was a Postdoctoral Research Associate with the Department of Electrical and Computer Systems Engineering. Monash University. He was also a Postdoctoral Research Fellow with the Faculty of Science, Engineering and Built Environment, Deakin University, Australia. His research interests include low power MEMS sensor interface circuits, mixed signal integrated circuit design, RF electronics, energy harvesting and biosensors for biomedical, and the Internet of Things applications.

NEMAI CHANDRA KARMAKAR (Senior Member, IEEE) received the B.Sc. degree in electrical and electronic engineering from the Bangladesh University of Engineering and Technology, the M.Sc. degree in electrical engineering from the University of Saskatchewan, Canada, and the Ph.D. degree in information technology and electrical engineering from The University of Queensland, St. Lucia, QLD, Australia, in 1999.

He is an Associate Professor with the Department of Electrical and Computer Systems Engineering, Monash University, Clayton, Australia. He has 20 years of teaching, design, and research experience in smart antennas, microwave active and passive circuits, and chipless RFIDs in both industry and academia in Australia, Canada, Singapore, and Bangladesh. He has authored and coauthored more than 230 refereed journal and conference papers, 24 refereed book chapters, and three edited and one coauthored books in RFID. His research interests include chipless RFID and RF sensors, smart antenna for mobile and satellite communication, planar phased array antennas, beamforming networks, and microwave device modelling.